Clim. Past Discuss., 8, 5263–5291, 2012
www.clim-past-discuss.net/8/5263/2012/
doi:10.5194/cpd-8-5263-2012

Climate of the Past Discussions

The Holocene thermal maximum in the Nordic Seas: the impact of Greenland Ice Sheet melt and other forcings in a coupled atmosphere-sea ice-ocean model

M. Blaschek and H. Renssen

Cluster Earth & Climate, Faculty of Earth and Life Sciences, VU University Amsterdam, De Boelelaan 1085, 1081HV Amsterdam, The Netherlands

Received: 3 October 2012 – Accepted: 19 October 2012 – Published: 26 October 2012

Correspondence to: M. Blaschek (m.blaschek@vu.nl)

Published by Copernicus Publications on behalf of the European Geosciences Union.

Abstract

The relatively warm early Holocene climate in the Nordic Seas, known as the Holocene Thermal Maximum (HTM), is often associated with an orbitally forced summer insolation maximum at 10 ka BP. The spatial and temporal response recorded in proxy data in the North Atlantic and the Nordic Seas reveal a complex interaction of mechanisms active in the HTM. Previous studies have investigated the impact of the Laurentide Ice Sheet (LIS), as a remnant from a previous glacial period, altering climate conditions with a continuous supply of melt water to the Labrador Sea and adjacent seas and with a downwind cooling effect from the remnant LIS. In our present work we extend this approach by investigating the impact of the Greenland Ice Sheet (GIS) on the early Holocene climate and the HTM. Reconstructions suggest melt rates of 13 mSv for 9 ka BP, which result in our model in a ocean surface cooling of up to 2 K near Greenland. Reconstructed summer SST gradients agree best with our simulation including GIS melt, confirming that the impact of early Holocene GIS is crucial for understanding the HTM characteristics in the Nordic Seas area. This implies that the modern and near-future GIS melt can be expected to play an active role in the climate system in the centuries to come.

1 Introduction

In the early Holocene a period of relatively warm climate, the Holocene thermal maximum (HTM), has been associated with the orbitally-forced Northern Hemisphere summer insolation maximum at approximately 10 ka BP (Jansen et al., 2008). Indeed, detailed analysis of proxy data and model results have confirmed that orbital forcing is the dominant long-term forcing considering temperature response at the scale of the Arctic (Renssen et al., 2009). Compared to this impact of orbital forcing, the effect of variations in the atmospheric greenhouse gases on the temperature response is relatively small (Renssen et al., 2009). Although the HTM is mainly orbitally forced, the spatial

CPD
8, 5263–5291, 2012

and temporal response of the climate system is diverse. Maximum temperatures were often delayed by several thousand years compared to the summer insolation maximum, as evidenced by numerous terrestrial and marine proxy records (e.g. Jansen et al., 2007). The causes of this spatial and temporal complexity of the HTM have not been resolved for all regions, for instance the Nordic Seas. In this paper we therefore evaluate the characteristics of the HTM in this important region by analysing the impact of potential forcing factors in numerical climate model simulations and by comparisons with available proxy evidence.

In a previous study, Renssen et al. (2009) have shown in transient climate model simulations, combined with summer temperature reconstructions based on terrestrial proxies, that the Laurentide Ice Sheet (LIS) delayed the HTM over the North Atlantic and down-wind continents by up to 3000 yr. This ice sheet persisted until around 6 ka BP, and caused regional cooling by inducing melt water discharges and by altering the surface albedo and topography. An important effect of the LIS melt flux was that it suppressed the deep convection in the Labrador Sea, causing expanded sea-ice cover and cool surface conditions compared to today. An important part of this spatio-temporal complexity can be explained by the impact of the remnant LIS in North America (Kaufman et al., 2004; Kaplan and Wolfe, 2006). However, the simulated characteristics of the HTM of Renssen et al. (2009) were not specifically compared to reconstructions of sea surface conditions, so that it remained unclear what the impact of the LIS was on modelled Holocene sea surface temperatures (SSTs) in the North Atlantic Ocean and the Nordic Seas, and if the model results were consistent with marine proxies from this region.

The characteristics of the HTM (timing and magnitude) in the Nordic Seas are rather unclear, as different marine proxies suggest different SST evolutions during the Holocene. Sea surface reconstructions based on diatoms show a non-uniform response of SSTs in the eastern and western parts of the Nordic Seas over the last 10 000 yr (Andersen et al., 2004). These diatom-based reconstructions indicate that over the Vøring Plateau (in the east), maximum warming occurred between 10 and

CPD
8, 5263–5291, 2012

9 ka BP, with summer SSTs being 4–5 K above the preindustrial mean, while on the western side the thermal maximum was later (between 8.5 and 6.5 ka BP) and less expressed (1 K above the preindustrial mean). Consequently, SSTs based on diatoms show an earlier (by 1.5–2.5 ka) and warmer HTM (3–4 K difference) on the eastern than on the western side. It has been suggested that the eastern side has a stronger response to orbital forcing in the early Holocene compared to the western side (Andersen et al., 2004). However, there has been quite some discussion of whether these warmer temperatures are due to insolation alone (Koç et al., 1993; Kaufman et al., 2004; Jansen et al., 2008; Risebrobakken et al., 2011). Eastern SSTs based on alkenones (Calvo et al., 2002) show a similar behaviour to the orbital trend, but are considerably lower at the thermal maximum (by 2–3 K) and yield a later HTM (i.e. between 8.5 and 5.5 ka BP) at the Vøring Plateau. Moreover, at the same site SST reconstructions based on foraminifera and radiolarians also lack this early HTM suggested by diatoms (Risebrobakken et al., 2003, 2011; Cortese et al., 2005; Dolven et al., 2002). Jansen et al. (2008) suggest that the SST maximum recorded in proxy data above the seasonal thermocline (diatoms, alkenones) is forced by the summer insolation maximum and deeper dwelling species (foraminifera and radiolarians) are not influenced. Andersson et al. (2010) support this hypothesis in a comparison with climate model simulations of the 6 ka BP climate performed with the CCSM3 model. These model results suggest that seasonal summer warming, related to the orbitally-forced summer insolation maximum, is restricted to the upper 30 m in the Nordic Seas during the early Holocene. Recently, Risebrobakken et al. (2011) separated the impact of orbitally-forced summer insolation and early Holocene warm surface waters associated with increased advection of Atlantic waters (Kaufman et al., 2004; Koç et al., 1993) and emphasized the involvement of more forcings than just radiative forcing to overall conditions in the Nordic Seas. Following this revision of early Holocene conditions, a non-uniform response across the Nordic Seas remains, although eastern SST reconstructions might be not as well known as previously anticipated, thus challenging

CPD
8, 5263–5291, 2012

the question of the origin of this zonal difference. Consequently, the expression of the HTM in the Nordic Seas and the impact of different forcing factors is still unclear.

In principle, climate model simulations could shed light on the role of different forcings and the SST response during the Holocene in the Nordic Seas. The model results of Renssen et al. (2009) suggest an earlier (8–7 ka BP) and warmer (more than 2 K above preindustrial level) thermal maximum in the western part of the Nordic Seas than in the eastern part (7–6 ka BP and up to 1 K above preindustrial level). Hence, these simulations did not capture the timing of the HTM and the gradient in the Nordic Seas as indicated by the diatom-based SST reconstructions. However, in the experiments of Renssen et al. (2009), the impact of the Greenland Ice Sheet (GIS) was not included, while potentially the sea surface conditions in the Western Nordic Seas were strongly influenced by GIS melt. It is likely that in the early Holocene the GIS was bigger than at present-day. Estimates from Peltier's (2004) ICE5G model suggest to a 25 % larger GIS at 9 ka BP, that loses mass until 7 ka BP and expands again before returning to its present-day extension at ~ 5 ka BP. Reconstructed GIS borehole site elevations from Vinther et al. (2009) suggest changes in the range of 100–300 m higher for 9 ka BP compared to today. Lower elevation sites like Camp Century and Dye3 show a fast decrease in elevation in the early Holocene, whereas NGRIP and GRIP give a steady decrease from the early to the late Holocene. Consequently, both these estimates support the idea that in the early Holocene the GIS melt flux was larger than today. No quantified estimates of this early Holocene melt flux have yet been published, but based on Peltier (2004) we could infer a best guess additional flux of 13 mSv ($1\ \mathrm{Sv} = 1 \times 10^6\ \mathrm{m^3\ s^{-1}}$) for 9 ka BP.

How does this early Holocene GIS melt flux compare to projections of GIS melt for the present and the near future? For the past two decades Rignot et al. (2011) find an acceleration of Greenland mass loss of 21.9 ± 1 $\mathrm{Gt\,yr^{-2}}$ (22 ± 4 $\mathrm{Gt\,yr^{-2}}$). Schrama and Wouters (2011), suggest 35 ± 1.5 cm of sea level rise associated with such GIS melt by 2100, resulting in a steady increase of melt water flux of up to 80 mSv at 2100. Using a climate model coupled to a dynamical GIS model, Driesschaert et al. (2007) simulate

CPD
8, 5263–5291, 2012

a future retreat of the GIS within 3000 yr under an extreme warming scenario, peaking with a relatively large melt rate of 0.1 Sv after 1000 yr, which has a noticeable weakening effect on the Atlantic Meridional Overturning Circulation (AMOC) in the model. However, when extrapolating the estimates from Rignot et al. (2011), such high melt rates would be reached soon after 2100 AD. Although these estimates assume a fixed acceleration rate, the comparison highlights the importance of the GIS in future and in warmer past climates.

Therefore, it is our objective in this paper to quantify the effect of GIS melt on the early Holocene climate in the Nordic Seas and to compare this impact with that of other important forcings by extending the modelling approach of Renssen et al. (2009). We present several transient simulations forcing our model with a transient LIS deglaciation and a GIS melt water flux derived from Peltier (2004). We use an updated version of the model (ECBilt-CLIO-VECODE) previously employed by Renssen et al. (2009). This model has now been renamed to LOVECLIM (Goosse et al., 2010). We focus on the expression of the HTM in the Nordic Seas and want to distinguish the impact of different forcings on SSTs. We will also evaluate what expression of SSTs in the Nordic Seas, as reconstructed using the different marine proxies, appears most consistent with our model results. In other words, does our model reproduce the clear east–west gradient and early timing of the HTM suggested by the diatom-based SST reconstructions, or rather a more uniform response across the Nordic Seas?

2 Experimental design

2.1 The model

We performed our experiments with the Earth system model of intermediate complexity (EMIC) LOVECLIM (version 1.2; Goosse et al., 2010), which includes a representation of the atmosphere, the ocean and sea-ice, the land-surface and its vegetation. We have not activated the components for dynamical ice sheets and the carbon cycle that are

CPD
8, 5263–5291, 2012

also included in LOVECLIM. We present here a brief summary of its key components, and more details can be found in Goosse et al. (2010). The sea-ice-ocean component is CLIO3 (Goosse and Fichefet, 1999), consisting of a free-surface ocean general circulation model with a horizontal resolution of 3 × 3 degrees latitude-longitude and 20 vertical levels, coupled to an sea-ice component (Fichefet and Maqueda, 1997, 1999) employing a three-layer dynamic-thermodynamic model that simulates a reasonably well present-day Arctic sea-ice distribution (Goosse et al., 2007). The atmospheric component is ECBILT (Opsteegh et al., 1998), a spectral T21, three-level quasi-geostrophic model including a bucket-type hydrological model for soil moisture and runoff. Cloud cover is climatologically prescribed. The vegetation is handled by VECODE (Brovkin et al., 2002) a dynamical vegetation model simulating two plant types, trees and grasses and desert as a dummy type. We prescribed the ice sheets manually. The climate sensitivity of LOVECLIM (version 1.2) to a doubling of the atmospheric CO_2 concentration is at the lower end of the range found in global climate models (1.9 K after 1000 yr; Goosse et al., 2010). The simulated deep ocean circulation in LOVECLIM1.2 compares reasonably well with other model results (Schmittner et al., 2005), with deep convection taking place in both the Nordic Seas and the Labrador Sea (Goosse et al., 2010). The model has been applied successfully in different palaeoclimatological modelling studies for settings like the 8.2 ka BP event (Wiersma and Renssen, 2006) and the Holocene (Renssen et al., 2009).

2.2 Experimental design

In this study we discuss the results of 4 transient experiments that cover the last 9000 yr and 8 quasi-equilibrium snapshot experiments, 7 with forcings fixed at 9 ka BP and 1 with forcings for the preindustrial era (Summary in Table 1). Except for the experiment with preindustrial forcings, the simulations were started at 9 ka BP because before that time the influence of the Younger Dryas cold period may still have an important influence on the climate through the long-term memory of the deep ocean. We forced all

CPD
8, 5263–5291, 2012

the simulations with orbital and greenhouse-gas concentrations in line with the PMIP3 protocol (http://pmip3.lsce.ipsl.fr). An overview of the forcings is provided in Fig. 1.

2.2.1 Snapshot experiments

We performed one control snapshot experiment for background conditions at 9 ka BP with orbital and greenhouse gas forcing (9kOG). This experiment was spun up for 1000 model years to ensure quasi-equilibrium conditions in all components of the model to the forcings (cf. Renssen et al., 2006). The final results of 9kOG have been used as initial conditions for all other 9k BP snapshot simulations, which have a duration of 500 model years during which the forcings were kept fixed. In PI and 9kOG, the land-sea-mask, the GIS topography, albedo, solar constant and aerosol content were fixed at PI configuration. The fixed land-sea mask will not likely impact the results as the difference in sea level between the two periods is only 19.71 m (9 ka BP; Siddall et al., 2003), implying that only a few grid cells are affected at the relatively low resolution of our model (i.e. T21 or about 560 km × 560 km in the horizontal grid space). Our analysis is based on averages that are calculated over the last 100 yr of the simulations.

We performed three 9 ka BP snapshot experiments to assess the sensitivity to the early Holocene GIS meltflux (Table 1, 9kOGx1, 9kOGx2, 9kOGx4). In these experiments, we prescribed multiples of a best-guess estimate of the early Holocene GIS melt flux of 13 mSv. This melt flux is derived from ice thickness changes provided at 500-yr time steps by Peltier (2004) ICE-5G model. We have added this melt water to the top layer of the ocean corresponding to the surface runoff outlets of the Greenland landmass.

In two additional snapshot experiments (9kOGMELT, 9kOGMELTICE) we added the LIS forcing to the impact of 9ka BP orbital and greenhouse forcing, identical to Renssen et al. (2009). In these experiments, we separately investigate the effect of an additional freshwater flux (0.09 Sv, denoted by MELT), representing the background melting of the LIS introduced at the St. Lawrence River outlet and Hudson Bay outlet, and the total effect of the remnant LIS (i.e. additional freshwater, albedo and topography

CPD
8, 5263–5291, 2012

changes) indicated by the name MELTICE. In agreement with paleoceanographic evidence (Hillaire-Marcel et al., 2001, 2007) Labrador Sea convection was suppressed by the LIS background melt flux.

Finally, we performed an equilibrium experiment (9kOGGIS) in which we combined all the forcings of the previous ones, and in addition included the best-guess GIS melt flux of 13 mSv.

2.2.2 Transient experiments

We performed one transient control simulation (OG) including only transient orbital and greenhouse gases and two transient simulations including additionally either LIS melt water (OGMELT) or the full LIS forcing (OGMELTICE). Following the setup of Renssen et al. (2009), the additional freshwater flux was set to 0.09 Sv between 9 to 8.4 ka BP, decreasing slightly to 0.08 Sv between 8.4 and 7.8 ka BP, dropping to 0.01 Sv between 7.8 and 6.8 ka BP (Fig. 1). These freshwater rates are based on adapted estimates by Licciardi et al. (1999). In OGMELTICE the effect of the disintegrating LIS was accounted for by changing the surface albedo and the topography at 50-yr time steps, interpolated from the reconstructions provided by Peltier (2004), during the period 9 to 7 ka BP.

Finally, we performed a transient experiment (OGGIS) that included the GIS melt water flux, in addition to all forcings prescribed in OGMELTICE. As shown in Fig. 1, the additional melt water was set to 13 mSv for 9 ka BP and increases to 23 mSv from 9 to 8 ka BP and then rapidly decreases to 3 mSv before vanishing completely at 7 ka BP (estimates derived from Peltier, 2004). Possible GIS topography changes in the model are fairly small in the model grid resolution (T21) and will be neglected.

Despite the imperfections in our reconstruction of the GIS, we argue that the amount of details provided reproduce a valid forcing for our model.

CPD
8, 5263–5291, 2012

3 Results and discussion

3.1 Early Holocene response

3.1.1 Simulated SSTs

Simulations including GIS melt (9kOGx1,2,4) show a clear August SST response near the southern part of Greenland, although the GIS melt is evenly distributed around Greenland. Compared to experiment 9kOG, in 9kOGx1 (Fig. 2a) melt water reduces SSTs around the southern tip of Greenland, especially the region near the Denmark Strait is affected, with lowest values at about −3 K. For a doubling of GIS melt (26 mSv) in experiment 9kOGx2 (Fig. 2b) the geographical pattern is quite similar to 9kOGx1 with a more pronounced cooling of up to 3 K near the Denmark Strait. Noticeable is also the development of a cold tongue across the Nordic Seas to the eastern side. Changes in 9kOGx4 (52 mSv, Fig. 2c) are hugely different from previous experiments. The core area of cooling is now in the Labrador Sea (more than 5 K) as the deep convection is locally shut down. This affects most of the North Atlantic as well as the Northern Nordic Seas.

In the early Holocene the Laurentide ice sheet puts great amounts (50 mSv in the Hudson Strait and 40 mSv in the St. Laurence Outlet) of freshwater into the adjacent ocean. In experiment 9kOGMELT (Fig. 2d) cooling due to this LIS melt water is affecting primarily the Labrador Sea with a cooling of up to 5 K. This cooling is due to the local shutdown of deep convection in the Labrador Sea, similar to what is seen here in 9kOGx4. However, compared to the latter experiment, there is less cooling impact on the rest of the North Atlantic and the Nordic Seas. Including the remnant ice sheet into experiment 9kOGMELTICE (Fig. 2e) further reduces SSTs (more than 6 K) in the Labrador Sea and enhances cooling down-wind of the ice sheet. Additional cooling affects the Northern Nordic Seas, whereas a more than 2 K warming appears in a small area in the Western Nordic Seas, near the Denmark Strait. Ultimately combining the LIS forcing with one time GIS melt (13 mSv) in experiment 9kOGGIS (Fig. 2f) further

CPD
8, 5263–5291, 2012

reduces Western Nordic Seas SSTs. Compared to 9kOGMELTICE, the warming near the Denmark Strait is reversed into a cooling that now expands across the Nordic Seas.

3.1.2 Comparison with proxy-based SSTs

Based on diatoms, Andersen et al. (2004) find a positive east–west August SST gradient of 5 to 6 K for the early Holocene, whereas using alkenone based summer SSTs (Calvo et al., 2002) for the eastern side yields a gradient of 3 to 4 K. We find in our experiment 9kOG a yearly gradient of ∼ 6 K and ∼ 4 K for August SSTs (Fig. 3). Modelling suggests zonal gradients are greatest in winter when the contrast between eastern and western water masses is greatest, as can be seen in Fig. 3 by February values of 7 to 8 K. Including GIS melt in 9kOGx1 increases August and annual SST gradient by 0.5 K compared to 9kOG. Experiment 9kOGx2 and 9kOGx4 reveal that a larger GIS melt leads to a slightly smaller east–west gradient, caused by an eastward spreading of the cold anomaly (compare with Fig. 2). In experiment 9kOGMELT the gradient is almost not affected compared to 9kOG, but in 9kOGMELTICE a clear reduction of the gradient is evident, with annual mean values around ∼ 4 K compared to 6 K in 9kOG. Along with this gradient reduction, a reduction in variability can be noted by smaller standard deviations. Finally, in 9kOGGIS the east–west SST gradient increases again to similar values as in 9kOGx1.

We find that GIS melt increases the east–west gradient and pushes the model climate more towards the proxy-based reconstructions. There is good agreement between simulated August SST gradients and reconstructed gradients for the diatom-alkenone combination (alkenone SST (east) minus diatom SST (west)). Alternatively we could argue for the just diatom gradient, but as eastern SSTs are not as high in the model as the reconstructed ones, we see the other possibility more likely. The gradient is strongest in winter. In conclusion, the better model-data fit in the experiments with the GIS melt indicates that it is important to include the GIS melt in simulations of the Holocene climate in the Nordic Seas. In other words, we propose that the impact of the GIS melt has been registered in the proxies, producing this increased SST gradient

CPD
8, 5263–5291, 2012

across the Nordic Seas in the early Holocene. Simulation 9kOGGIS is therefore the best estimate for the early Holocene climate in our model. Regarding the foraminifera-based SSTs, our model shows that seasonal summer warming in the early Holocene is mainly active in the upper ∼100 m (not shown), in line with findings from Andersson et al. (2010) for the Mid-Holocene. Our model further shows that GIS melt affects only the first 50 m of the ocean column (not shown). Therefore, it is likely that deeper dwelling foraminifera species should be less affected by orbitally-forced summer warming and GIS melt compared to surface dwellers.

3.1.3 Mechanisms behind SST patterns

As discussed in Sect. 3.1.1, we have simulated clear cooling patterns in the Labrador Sea, the Irminger Sea and the Nordic Seas. What has caused these cooling patterns? In our simulations we find the impacts of the following forcings on August SSTs: (1) GIS melt near Greenland, (2) LIS melt water in the Labrador Sea, (3) the remnant LIS, (4) the combined effect of LIS and GIS. Connected to these impacts are also different mechanisms like (1) reduced vertical heat transfer, (2) sea-ice growth and stratification of the ocean and therefore inhibiting convection, (3) downwind atmospheric cooling from a large ice-sheet.

The pattern found in SSTs from Greenland melt water (Fig. 2a, b, 9kOGx1, 2) is a result of freshening and stratifying of the upper ocean. Surface waters become more buoyant and the density gradient with the subsurface increases (up to 0.18 $kg\,m^{-3}$ from 5 to 100 m depth for 9kOGx1), thus reducing upward vertical heat transfer and causing surface cooling. In general, the southern tip of Greenland is where the freshwater (runoff, sea-ice) from the Arctic and Greenland results in the largest cooling in 9kOGx1 and 9kOGx2. In the Arctic Ocean, however, surface waters are already quite fresh and stratified, minimizing the effect of additional melt water. As a consequence of cooler and fresher surface waters, sea-ice growth is facilitated here and local convection in winter is reduced (9kOGx1 by up to −200 m of maximum convection depth relative to 9kOG,assisting in an overall cooling effect.

CPD
8, 5263–5291, 2012

Considering the combined effect of all mentioned forcings (by comparing 9kOGGIS to 9kOG), the Northern Hemisphere sea-ice area and volume increase by up to 18 % and 28 % (Table 2), respectively, with the biggest changes in Labrador Sea area, while the increases are minor in the Nordic Seas. The strong cooling in the Labrador Sea are linked to local collapse of deep convection and expansion of sea-ice cover occurring due to strong surface freshening here. In 9kOGGIS this freshening is primarily resulting from the LIS melt (c.f. Renssen et al., 2005, 2009), but the same effect is seen when the GIS melt is increased, as in 9kOGx4 (Fig. 2c). The absence of deep convection in the Labrador Sea results in a reduction of meridional overturning strength in the North Atlantic. The simulated deep ocean circulation for 9kOG has a maximum overturning stream function in the North Atlantic of 22 ± 1.3 Sv and an export of NADW towards the Southern Ocean of 12 ± 0.8 Sv. In this experiment, deep convection takes place in both the Nordic Seas and the Labrador Sea, similar to the conditions in a simulation with pre-industrial forcings (Goosse et al., 2010). In our experiments the GIS melt has a discernible impact on convection depth near the Denmark Strait which is contributing to the North Atlantic overturning. In 9kOGx1 a reduction of ∼ 9 % (19.8 Sv vs 21.6 Sv, Table 2) of the maximum meridional overturning strength is simulated compared to 9kOG. As expected, this weakening of the AMOC is enhanced when also LIS melt is included, resulting in similarly reduced values of the maximum meridional overturning strength in 9kOGMELTICE (15.6 Sv) and in 9kOGGIS (14.5 Sv). This results in an reduced annual northward heat transport at 30° S in the North Atlantic basin of 68 % for 9kOGGIS (0.127 PW) compared to 9kOG (0.214 PW), contributing to the cooling of the Northern Hemisphere. This is best expressed in 9kOGx4 (∼ 71 % reduction) and 9kOGMELT (∼ 62 % reduction), as in these experiments the impact on meridional overturning strength is the largest.

Another superimposed effect contributes to cooler North Atlantic SSTs in 9kOGMELTICE and 9kOGGIS, which is the enhanced cooling (by 2 K in 9kOGICE vs 0.5 K in 9kOGMELT, Figs 2e, f) downwind of the remnant LIS as discussed in detail in Renssen et al. (2009). Meridional overturning in the Nordic Seas and therefore NAC strength

CPD
8, 5263–5291, 2012

are weakly affected (cf. Table 2) by overall cooling and freshening (2.65 Sv in OGGIS vs 2.78 Sv in OG), because of their competing effects on surface density and therefore convective activity. In the Nordic Seas at the main deep convection site South of Svalbard, the freshening is relatively modest (compared to the Labrador Sea). The reduction in the surface density resulting from this freshening is almost compensated by the increase in density caused by the surface cooling. As a consequence, maximum winter convection depth is only reduced by 200 m in 9kOGGIS compared to 9kOG at the convection site.

3.2 Transient Holocene response

From our snapshot simulations we could derive a discernible response to GIS melt, that seems to be also visible in the proxy-based reconstructions and is denoted by an early Holocene increased August SST gradient across the Nordic Seas. Therefore we want to investigate the temporal evolution of this impact on the HTM.

3.2.1 Simulated SST trends

Modelled Nordic Seas SST gradient responds stronger to GIS melt water than to effects inflicted by the remnant Laurentide ice sheet. The Eastern Nordic Seas SSTs in OG show a clear early (before 8 ka BP) HTM and a subsequent decline towards preindustrial temperatures. Inducing the LIS melt water in OGMELT, affects that part of the Nordic Seas only minor (less than 0.5 K difference). Whereas in OGMELTICE, the additional remnant ice sheet reduces SSTs by 1.5 K in the early Holocene (Fig. 4a) relative to OG. With the ice sheet vanishing at around 7 ka BP, temperatures return to the general orbitally-forced trend during the remainder of the Holocene, depicted by simulation OG. The GIS melt affects previously mentioned results only in the first 500 yr, when GIS melt is at its top, causing warmer conditions by 0.5 K. In contrast, SSTs in the Western Nordic Seas (Fig. 4b) are stronger reduced by GIS melt (by $\sim$3 K) in OGGIS than by the influence of the LIS in OGMELTICE ($\sim$2 K). This impact wears off at 7.5 ka BP,

CPD
8, 5263–5291, 2012

when temperatures return to the general trend displayed by OG. As a consequence of the noted different effects in the Western and Eastern Nordic Seas, the gradient across the Nordic Seas is more strongly influenced by GIS melt and less so by the remnant LIS. We can clearly see in Fig. 4c the impact of GIS melt on the spatial SST pattern in the Nordic Seas, because simulated SSTs for East and West decrease over time, the gradient is constant over most of the Holocene, but in the early Holocene (before 7.5 ka BP) the east–west gradient is clearly steeper in OGGIS than in OGMELTICE, reflecting the strong impact of the GIS melt. As soon as GIS melt vanishes, this gradient in OGGIS returns to the same level as the other experiments, suggesting that in order to reproduce a gradual, more proxy-like decrease of that spatial gradient, the GIS melt water should have been longer active. Alternatively, another yet unknown forcing might have caused the prolonged cooling of the Western Nordic Seas, as in any case it seems to be clear that the impact has to be on the western side, rather than on the eastern side.

3.2.2 Impact on the HTM

The spatial pattern of the HTM timing is mainly influenced by the remnant LIS and secondly, but fundamentally in the Nordic Seas, by the GIS melt (Fig. 5). Our main interest here is in the millennial-scale trend. Therefore, to filter out decadal-centennial variability, we used a 1000 yr running mean. We calculated the timing (in yr BP) of the maximum for August SSTs. Relative to OG, peak warmth is delayed by up to 3500 yr in the Nordic Seas and is highly variable between the four transient simulations. In OGMELT, the LIS delays the timing of the HTM over the whole North Atlantic by ~ 1000 yr (Fig. 5a, b). The Denmark Strait and the region south show HTM timings of ~ 2000 yr later than in OG. A major step happens by including the remnant ice sheet in OGMELTICE, which further increases the timing delay to 2000–2500 yr for big parts of the North Atlantic. The Eastern Nordic Seas are delayed by 2000 yr, whereas the western range by 500 to 2500 yr, suggesting a west-east spatial timing gradient, rather than a east–west gradient. Including the GIS melt in OGGIS uniformly delays the western

CPD
8, 5263–5291, 2012

side, resulting in a spatial timing gradient of 2000 yr across the Nordic Seas. It should be noted that the HTM timing in our transient experiment depends strongly on the timescale of the applied forcings. Therefore, it is preferable to consider the relative timings (i.e. timing delays compared to orbital and freshwater forcing) when comparing with proxy data (Sect. 3.2.3).

3.2.3 Proxy trends and timings

Despite uncertainties in model and proxy results the combination of LIS and GIS forcings link reconstructed to modelled estimates of SST trends and timing of the HTM. The zonal Nordic Seas SST gradient in Andersen et al. (2004) decreases more continuously than our associated model SST gradient. However, given the step-like nature of our prescribed melt fluxes an abrupt termination is inevitable. Reconstructed proxy SST trends over the last 9000 yr from Andersen et al. (2004) are 5 K (eastern) compared to 1–2 K for the model and 1–2 K (western) compared to 1 K for the model. Slightly better are SST trends from Calvo et al. (2002) with 2–3 K compared to 1–2 K for the model. Marine sites from Kaufman et al. (2004) in the Nordic Seas give SST trends between 2.5 and 6.6 K, mostly being diatoms. Despite this weak consistency in absolute temperatures, the proxies give gradients that vary more (between ∼2 K for present-day and ∼6–8 K for the early Holocene (Calvo et al., 2002; Andersen et al., 2004) compared to the model gradient (2.5–4.5 for present-day and ∼5 K for the early Holocene), but leave some similarities.

The spatial complexity of the HTM is best expressed by estimating delays and spatial timing differences. From Kaufman et al. (2004) a timing for the HTM at the Eastern Greenland shelf ranges between 9 and 5 ka BP, translating into a 0 to 4 ka delay. At the South Iceland shelf the timing is between 7 and 6 ka BP according to Kaufman et al. (2004), whereas the North Iceland shelf is between 9 and 6 ka BP, resulting in delay between 0 and 3 ka and a spatial timing gradient of 0 to 2 ka. Similar results can be obtained from Andersen et al. (2004) for Greenland and Iceland sites, however for the Norwegian site the timing delay is ∼1 ka BP.

CPD
8, 5263–5291, 2012

Our model results for OGGIS seem to be in the range for most of these timing differences, except the spatial difference between North and South Iceland is unmatched. We find it reversed.

4 Conclusions

We have applied a fully coupled atmosphere-ocean-sea-ice-vegetation model to study the impact of early Holocene GIS melt on the climate of the Nordic Seas. Our results suggest the following.

1. From our sensitivity experiments we find that GIS melt has a discernible impact on the AMOC strength and facilitates sea-ice growth along the EGC and the Denmark Strait. August SSTs are up to 3 K lower near the Denmark Strait, overturning is reduced by 2–3 Sv and winter sea-ice margin expands south of Denmark Strait in a simulation with 13 mSv GIS melt.

2. GIS melt can explain some of the spatial gradients across the Nordic Seas as reconstructed in several proxy records for the early Holocene. Although absolute model temperatures do not compare well with exact core locations, because of the coarse resolution of our model, but the model seems to catch well the spatial gradient across the Nordic Seas. Our model was not able to reproduce the warmth in the early Holocene as suggested by diatom reconstructions near the Norwegian Shelf and agrees better with Alkenone derived sea-surface temperatures.

3. The spatial distribution of the timing of the HTM in the Nordic Seas is better reproduced in a simulation with GIS melt. We find delays between eastern and western side of $\sim$2000 yr.

4. We find in our experiments that GIS melt plays an active role in the Nordic Seas environment and GIS evolution therefore has to be considered in the evolution of the early Holocene climate and future melting scenarios. Global radiative forcing

CPD
8, 5263–5291, 2012

based on future anthropogenic emission scenarios vary between ∼3 and ∼8.5 $W m^{-2}$ (Meinshausen et al., 2011) whereas at 65° N, in South Greenland, the annual forcing was ∼2.4 $W m^{-2}$ and ∼42 $W m^{-2}$ in summer (Berger and Loutre, 1991) at 9 ka BP in the early Holocene. So it is not surprising that recently Rignot et al. (2011) reported an acceleration of GIS melt rates that could soon outrange those of the early Holocene, and thereby stressing the importance of GIS melt for Nordic Seas future climate evolution.

Acknowledgements. This work was supported by funding of the "European Community's 7th Framework Programme FP7 2007/2013, Marie-Curie Actions, under Grant Agreement No. 238111" CASE ITN. This support is gratefully acknowledged.

References

Andersen, C., Koç, N., Jennings, A., and Andrews, J. T.: Nonuniform response of the major surface currents in the Nordic Seas to insolation forcing: implications for the Holocene climate variability, Paleoceanography, 19, PA2003, doi:10.1029/2002PA000873, 2004. 5265, 5266, 5273, 5278

Andersson, C., Pausata, F. S. R., Jansen, E., Risebrobakken, B., and Telford, R. J.: Holocene trends in the foraminifer record from the Norwegian Sea and the North Atlantic Ocean, Clim. Past, 6, 179–193, doi:10.5194/cp-6-179-2010, 2010. 5266, 5274

Berger, A. and Loutre, M.: Insolation values for the climate of the last 10 million years, Quaternary Sci. Rev., 10, 297–317, doi:10.1016/0277-3791(91)90033-Q, 1991. 5280, 5287

Brovkin, V., Bendtsen, J., Claussen, M., Ganopolski, A., Kubatzki, C., Petoukhov, V., and Andreev, A.: Carbon cycle, vegetation, and climate dynamics in the Holocene: experiments with the CLIMBER-2 model, Global Biogeochem. Cy., 16, 1139, doi:10.1029/2001GB001662, 2002. 5269

Calvo, E., Grimalt, J., and Jansen, E.: High resolution U37K sea surface temperature reconstruction in the Norwegian Sea during the Holocene, Quaternary Sci. Rev., 21, 1385–1394, doi:10.1016/S0277-3791(01)00096-8, 2002. 5266, 5273, 5278

Cortese, G., Dolven, J. K., Bjørklund, K. R., and Malmgren, B. A.: Late Pleistocene–Holocene radiolarian paleotemperatures in the Norwegian Sea based on artificial neural networks, Palaeogeogr. Palaeocl., 224, 311–332, doi:10.1016/j.palaeo.2005.04.015, 2005. 5266

Dolven, J. K., Cortese, G., and Bjørklund, K. R.: A high-resolution radiolarian-derived paleotemperature record for the Late Pleistocene-Holocene in the Norwegian Sea, Paleoceanography, 17, 1072, doi:10.1029/2002PA000780, 2002. 5266

Driesschaert, E., Fichefet, T., Goosse, H., Huybrechts, P., Janssens, I., Mouchet, A., Munhoven, G., Brovkin, V., and Weber, S. L.: Modeling the influence of Greenland ice sheet melting on the Atlantic meridional overturning circulation during the next millennia, Geophys. Res. Lett., 34, L10707, doi:10.1029/2007GL029516, 2007. 5267

Fichefet, T. and Maqueda, M. A. M.: Sensitivity of a global sea ice model to the treatment of ice thermodynamics and dynamics, J. Geophys. Res., 102, 12609–12646, doi:10.1029/97JC00480, 1997. 5269

Fichefet, T. and Maqueda, M. A. M.: Modelling the influence of snow accumulation and snow-ice formation on the seasonal cycle of the Antarctic sea-ice cover, Clim. Dynam., 15, 251–268, doi:10.1007/s003820050280, 1999. 5269

Goosse, H. and Fichefet, T.: Importance of ice-ocean interactions for the global ocean circulation: a model study, J. Geophys. Res., 104, 23337–23355, doi:10.1029/1999JC900215, 1999. 5269

Goosse, H., Driesschaert, E., Fichefet, T., and Loutre, M.-F.: Information on the early Holocene climate constrains the summer sea ice projections for the 21st century, Clim. Past, 3, 683–692, doi:10.5194/cp-3-683-2007, 2007. 5269

Goosse, H., Brovkin, V., Fichefet, T., Haarsma, R., Huybrechts, P., Jongma, J., Mouchet, A., Selten, F., Barriat, P.-Y., Campin, J.-M., Deleersnijder, E., Driesschaert, E., Goelzer, H., Janssens, I., Loutre, M.-F., Morales Maqueda, M. A., Opsteegh, T., Mathieu, P.-P., Munhoven, G., Pettersson, E. J., Renssen, H., Roche, D. M., Schaeffer, M., Tartinville, B., Timmermann, A., and Weber, S. L.: Description of the Earth system model of intermediate complexity LOVECLIM version 1.2, Geosci. Model Dev., 3, 603–633, doi:10.5194/gmd-3-603-2010, 2010. 5268, 5269, 5275

Hillaire-Marcel, C., de Vernal, A., Bilodeau, G., and Weaver, A. J.: Absence of deep-water formation in the Labrador Sea during the last interglacial period, Nature, 410, 1073–1077, doi:10.1038/35074059, 2001. 5271

CPD
8, 5263–5291, 2012

Hillaire-Marcel, C., de Vernal, A., and Piper, D. J. W.: Lake Agassiz Final drainage event in the northwest North Atlantic, Geophys. Res. Lett., 34, L15601, doi:10.1029/2007GL030396, 2007. 5271

IPCC: Climate Change: The Scientific Basis, Chap. 6, 349–416, Cambridge University Press, Cambridge, UK and New York, NY, USA, 2001. 5287

Jansen, E., Overpeck, J., Briffa, K., Duplessy, J.-C., Joos, F., Masson-Delmotte, V., Olago, D., Otto-Bliesner, B., Peltier, W., Rahmstorf, S., Ramesh, R., Raynaud, D., Rind, D., Solomina, O., Villalba, R., and Zhang, D.: Palaeoclimate, in: Climate Change 2007: The Physical Science Basis, available at: http://www.ipcc.ch/publications_and_data/ar4/wg1/en/ch6.html (last access: 24 October 2012), 2007. 5265

Jansen, E., Andersson, C., Moros, M., Nisancioglu, K. H., Nyland, B. F., and Telford, R. J.: The early to mid-Holocene thermal optimum in the North Atlantic, Wiley Blackwell, in: Natural Climate Variability and Global Warming: A Holocene Perspective, doi:10.1002/9781444300932.ch5, 123–137, 2008. 5264, 5266

Kaplan, M. R. and Wolfe, A. P.: Spatial and temporal variability of Holocene temperature in the North Atlantic region, Quaternary Res., 65, 223–231, doi:10.1016/j.yqres.2005.08.020, 2006. 5265

Kaufman, D., Ager, T., Anderson, N., Anderson, P., Andrews, J., Bartlein, P., Brubaker, L., Coats, L., Cwynar, L., Duvall, M., Dyke, A., Edwards, M., Eisner, W., Gajewski, K., Geirsdóttir, A., Hu, F., Jennings, A., Kaplan, M., Kerwin, M., Lozhkin, A., MacDonald, G., Miller, G., Mock, C., Oswald, W., Otto-Bliesner, B., Porinchu, D., Rühland, K., Smol, J., Steig, E., and Wolfe, B.: Holocene thermal maximum in the Western Arctic (0–180°W), Quaternary Sci. Rev., 23, 529–560, doi:10.1016/j.quascirev.2003.09.007, 2004. 5265, 5266, 5278

Koç, N., Jansen, E., and Haflidason, H.: Paleoceanographic reconstructions of surface ocean conditions in the Greenland, Iceland and Norwegian seas through the last 14 ka based on diatoms, Quaternary Sci. Rev., 12, 115–140, doi:10.1016/0277-3791(93)90012-B, 1993. 5266

Licciardi, J. M., Teller, J. T., and Clark, P. U.: Freshwater routing by the Laurentide Ice Sheet during the last deglaciation, in: Mechanisms of Global Climate Change at Millennial Time Scales, edited by: Clark, P., Webb, R., and Keigwin, L., 112, Geophys. Monogr. Ser., Amer. Geophys. Union, Washington DC, 177–201, available at: http://www.unh.edu/esci/people/pdf/licciardi_et-al-1999-agu.pdf, 1999. 5271, 5285

CPD
8, 5263–5291, 2012

Meinshausen, M., Smith, S., Calvin, K., Daniel, J., Kainuma, M., Lamarque, J.-F., Matsumoto, K., Montzka, S., Raper, S., Riahi, K., Thomson, A., Velders, G., and van Vuuren, D.: The RCP greenhouse gas concentrations and their extensions from 1765 to 2300, Climatic Change, 109, 213–241, doi:10.1007/s10584-011-0156-z, 2011. 5280

Opsteegh, J. D., Haarsma, R. J., Selten, F. M., and Kattenberg, A.: ECBILT: a dynamic alternative to mixed boundary conditions in ocean models, Tellus A, 50, 348–367, doi:10.1034/j.1600-0870.1998.t01-1-00007.x, 1998. 5269

Peltier, W.: Global glacial isostasy and the surface of the Ice-age Earth: the ICE-5G (VM2) model and grace, Annu. Rev. Earth Pl. Sc., 32, 111–149, doi:10.1146/annurev.earth.32.082503.144359, 2004. 5267, 5268, 5270, 5271, 5285, 5287

Renssen, H., Goosse, H., Fichefet, T., Brovkin, V., Driesschaert, E., and Wolk, F.: Simulating the Holocene climate evolution at northern high latitudes using a coupled atmosphere-sea ice-ocean-vegetation model, Clim. Dynam., 24, 23–43, doi:10.1007/s00382-004-0485-y, 2005.

Renssen, H., Goosse, H., and Muscheler, R.: Coupled climate model simulation of Holocene cooling events: oceanic feedback amplifies solar forcing, Clim. Past, 2, 79–90, doi:10.5194/cp-2-79-2006, 2006.

Renssen, H., Seppa, H., Heiri, O., Roche, D. M., Goosse, H., and Fichefet, T.: The spatial and temporal complexity of the Holocene thermal maximum, Nat. Geosci., 2, 411–414, doi:10.1038/ngeo513, 2009. 5264, 5265, 5267, 5268, 5269, 5270, 5271, 5275

Rignot, E., Velicogna, I., van den Broeke, M. R., Monaghan, A., and Lenaerts, J.: Acceleration of the contribution of the Greenland and Antarctic ice sheets to sea level rise, Geophys. Res. Lett., 38, L05503, doi:10.1029/2011GL046583, 2011. 5267, 5268, 5280

Risebrobakken, B., Jansen, E., Andersson, C., Mjelde, E., and Hevrøy, K.: A high-resolution study of Holocene paleoclimatic and paleoceanographic changes in the Nordic Seas, Paleoceanography, 18, 1017, doi:10.1029/2002PA000764, 2003. 5266

Risebrobakken, B., Dokken, T., Smedsrud, L. H., Andersson, C., Jansen, E., Moros, M., and Ivanova, E. V.: Early Holocene temperature variability in the Nordic Seas: the role of oceanic heat advection versus changes in orbital forcing, Paleoceanography, 26, PA4206, doi:10.1029/2011PA002117, 2011. 5266

Schmittner, A., Latif, M., and Schneider, B.: Model projections of the North Atlantic thermohaline circulation for the 21st century assessed by observations, Geophys. Res. Lett., 32, L23710, doi:10.1029/2005GL024368, 2005. 5269

CPD
8, 5263–5291, 2012

Schrama, E. J. O. and Wouters, B.: Revisiting Greenland ice sheet mass loss observed by GRACE, J. Geophys. Res., 116, B02407, doi:10.1029/2009JB006847, 2011. 5267

Siddall, M., Rohling, E. J., Almogi-Labin, A., Hemleben, C., Meischner, D., Schmelzer, I., and Smeed, D. A.: Sea-level fluctuations during the last glacial cycle, Nature, 423, 853–858, doi:10.1038/nature01690, 2003.

Vinther, B. M., Buchardt, S. L., Clausen, H. B., Dahl-Jensen, D., Johnsen, S. J., Fisher, D. A., Koerner, R. M., Raynaud, D., Lipenkov, V., Andersen, K. K., Blunier, T., Rasmussen, S. O., Steffensen, J. P., and Svensson, A. M.: Holocene thinning of the Greenland ice sheet, Nature, 461, 385–388, doi:10.1038/nature08355, 2009. 5267

Wiersma, A. and Renssen, H.: Model-data comparison for the 8.2 ka BP event: confirmation of a forcing mechanism by catastrophic drainage of Laurentide Lakes, Quaternary Sci. Rev., 25, 63–88, doi:10.1016/j.quascirev.2005.07.009, 2006. 5269

CPD
8, 5263–5291, 2012

Table 1. Summary of the experimental design. Transient forcings are shown in Fig. 1. Orbital parameters and Greenhouse Gases are in line with the PMIP3 protocol (http://pmip3.lsce.ipsl.fr/) for transient simulations. Laurentide Ice sheet melt water fluxes are from Licciardi et al. (1999). Greenland Ice Sheet melt water fluxes are calculated from Peltier (2004) ice thickness changes.

Experiment name	Initial conditions	GIS Melt flux (Sv)	LIS Melt flux (Sv)
9kOG	Orbital (9000 BP), greenhouse gases (9000 BP)	0	0
PI	Orbital (1950 AD), greenhouse gases (1750 AD)	0	0
9kOGx1	9kOG+ Greenland ice sheet melt	0.013	0
9kOGx2	9kOG+ Greenland ice sheet melt	0.026	0
9kOGx4	9kOG+ Greenland ice sheet melt	0.052	0
9kOGMELT	9kOG+ Laurentide Ice Sheet melt water	0	0.09
9kOGMELTICE	9kOGMELT + ice sheet (albedo + topography)	0	0.09
9kOGGIS	9kOGMELTICE + GIS melt water	0.013	0.09
OG	Transient orbital and greenhouse gases (9–0 ka BP) from PMIP3 transient simulation setup	0	0
OGMELT	OG + Laurentide Ice Sheet melt water	0	0
OGICE	OGMELT + ice sheet (albedo + topography)	0	0.09 – 0
OGGIS	OGICE + GIS melt water	0.026 – 0	0.09 – 0

CPD
8, 5263–5291, 2012

Table 2. Summary table of snapshot simulations for meridional overturning circulation in the Nordic Seas, the North Atlantic, Sea Ice area and volume in the Northern Hemisphere, North Atlantic Current (NAC) strength, Meridional heat flux in the ocean at 30° S and east–west August SST Gradient for different simulations. Calculated from the last 100 yr of the experiments. Shown are means and standard deviations (sd). Bold numbers are outside the range of mean and 1 standard deviation of simulation OG.

	Convection				Sea Ice			
	Nordic Seas (Sv)		North Atlantic (Sv)		Area (10^6 km^2)		Volume (10^3 km^3)	
OG	2.78	± 0.15	21.63	± 1.33	8.80	± 0.24	8.86	± 0.62
9kOGGISx1	2.80	± 0.15	**19.78**	± 0.96	8.94	± 0.22	9.00	± 0.52
9kOGGISx2	2.88	± 0.16	**18.71**	± 0.57	9.00	± 0.26	9.16	± 0.60
9kOGGISx4	2.72	± 0.28	**13.54**	± 0.44	**9.72**	± 0.41	**10.06**	± 0.88
OGMELT	2.75	± 0.17	**13.61**	± 0.47	**9.58**	± 0.30	**9.87**	± 0.79
OGMELTICE	**2.53**	± 0.21	**15.66**	± 0.54	**10.26**	± 0.29	**11.29**	± 0.80
OGGIS	2.65	± 0.19	**14.49**	± 0.72	**10.37**	± 0.26	**11.36**	± 0.71

	NAC Strength (Sv)		Meridional Heat Flux 30° S (PW)		East–West Gradient August SST (K)	
OG	9.78	± 0.50	0.214	± 0.042	3.82	± 0.60
9kOGGISx1	9.81	± 0.47	0.194	± 0.032	4.39	± 0.57
9kOGGISx2	9.55	± 0.42	0.194	± 0.036	4.25	± 0.53
9kOGGISx4	9.66	± 0.63	**0.125**	± 0.045	4.08	± 0.87
OGMELT	9.41	± 0.67	**0.132**	± 0.045	4.07	± 0.81
OGMELTICE	9.60	± 0.74	**0.136**	± 0.050	**2.80**	± 0.88
OGGIS	9.52	± 0.56	**0.127**	± 0.044	**4.51**	± 1.05

CPD
8, 5263–5291, 2012

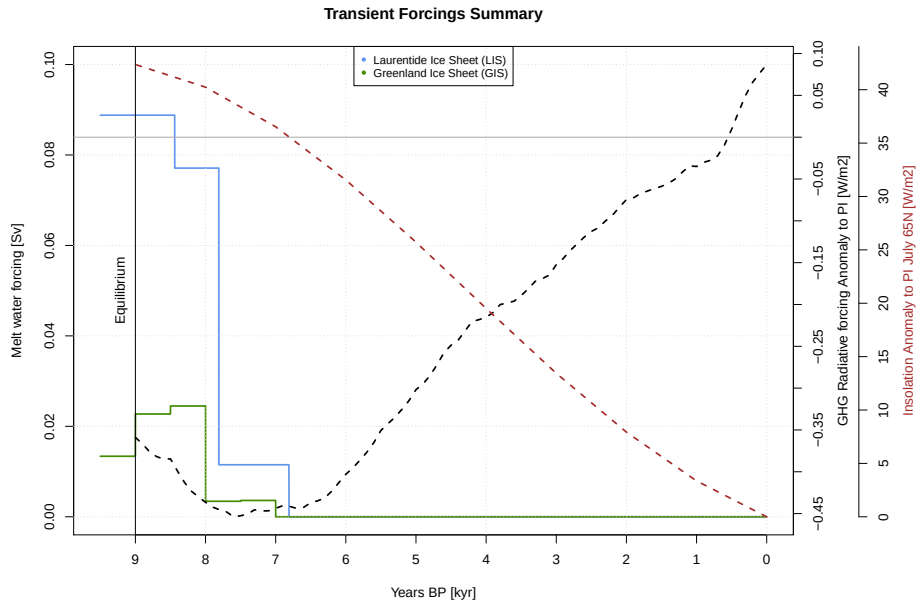

Fig. 1. Melt water forcing applied in transient simulations. Blue is the total LIS melt water flux applied in all OGICE Simulations. The Green curve denotes the calculated GIS melt water from Peltier (2004) used in OGGIS. Black gives the radiative forcing due to greenhouse gas concentrations and the red curve gives the July 65° N insolation anomaly after Berger and Loutre (1991). Greenhouse gas radiative forcing is calculated using IPCC (2001) formulation.

CPD
8, 5263–5291, 2012

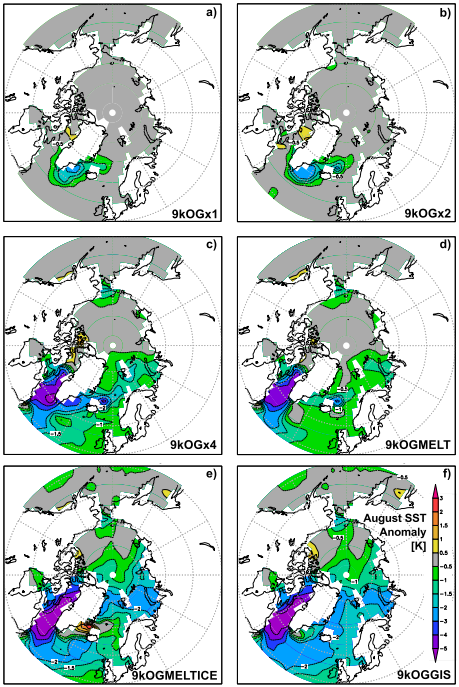

Fig. 2. Sea Surface Temperature (SST, scale in K) anomaly compared to OG for 9 ka BP snapshot simulations. **(a)** 9kOGx1 SST anomaly for GIS melt (13mSv). **(b)** 9kOGx2 SST anomaly for GIS melt (26 mSv). **(c)** 9kOGx4 SST anomaly for GIS melt (52 mSv). **(d)** 9kOGMELT SST anomaly for LIS melt (0.09 Sv). **(e)** 9kOGMELTICE SST anomaly for LIS melt (0.09Sv) + remnant ice sheet (albedo + topography). **(f)** 9kOGGIS SST anomaly for LIS melt + remnant ice sheet + additional GIS melt (13 mSv).

CPD
8, 5263–5291, 2012

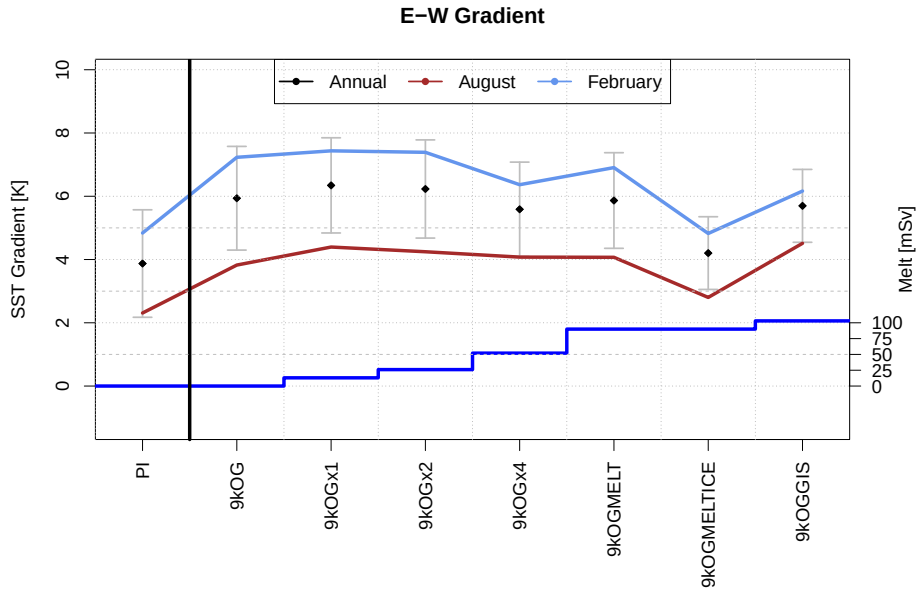

Fig. 3. Simulated SST east–west gradients across the Nordic Seas for 9 ka BP snapshot simulations and an additional present day (PI) simulation for comparison. Corresponding eastern model area 47.5–10° W, 68.75–81.25° N and western 2.5–20° E, 66.25–78.75° N. Points mark the annual mean gradient, grey bars give associated standard deviation, red line gives August value, light blue line gives February value. Dark blue line at the bottom gives the total amount of freshwater added to the simulations in mSv.

CPD
8, 5263–5291, 2012

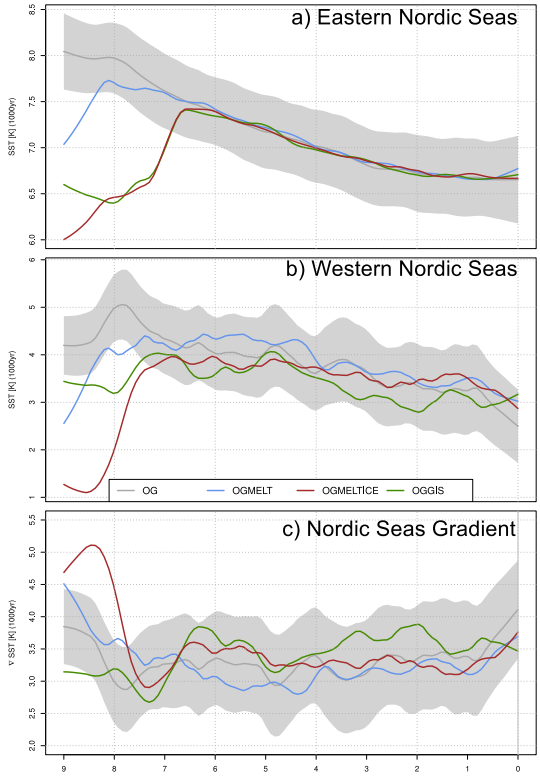

Fig. 4. Transient area weighted SSTs and gradient for Eastern and Western Nordic Seas from four transient simulations. **(a)** August SST in the Eastern Nordic Seas (2.5–20° E, 66.25–78.75° N) from 9 to 0 ka BP. **(b)** August SST in the Western Nordic Seas (47.5–10° W, 68.75–81.25° N) from 9 to 0 ka BP. **(c)** August SST east–west gradient in the Nordic Seas from 9 to 0 ka BP. Grey OG, Blue OGMELT, Red OGMELTICE and Green OGGIS.

CPD
8, 5263–5291, 2012

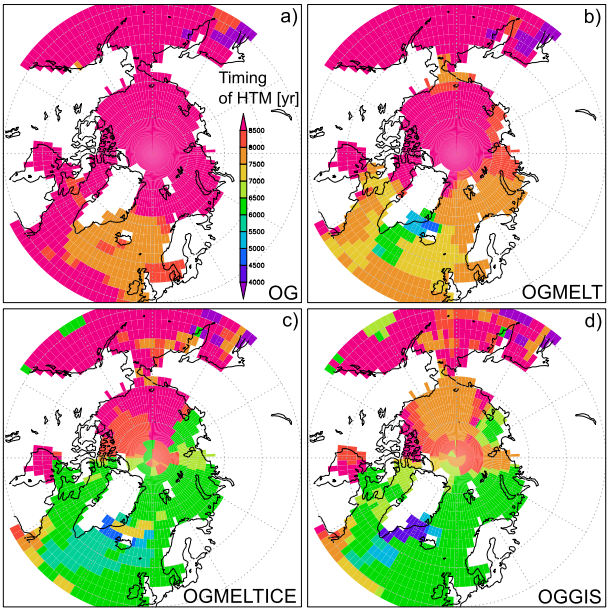

Fig. 5. Calculated timing of the Holocene Thermal Maximum (in yr BP) based on simulated August SSTs in the Northern Hemisphere (in yr) for four transient simulations. Temperatures have been filtered with a 1000 yr running mean. **(a)** OG; **(b)** OGMELT; **(c)** OGMELTICE; **(d)** OGGIS.

CPD
8, 5263–5291, 2012